Y$_{1-x}$La$_x$VO$_3$: Effects of doping on orbital ordering

S. Yano,[1] Despina Louca,[1] J. C. Neuefeind,[2] J.-Q. Yan,[2,3] J.-S. Zhou,[4] and J. B. Goodenough[4]

[1]*University of Virginia, Charlottesville, Virginia 22904, USA*
[2]*Oak Ridge National Laboratory, Oak Ridge, Tennessee 37831, USA*
[3]*University of Tennessee, Knoxville, Tennessee 37996, USA*
[4]*University of Texas at Austin, Austin, Texas 78712, USA*

The effects of isovalent doping on orbital ordering in the perovskite Y$_{1-x}$La$_x$VO$_3$ were investigated using neutron diffraction and the pair distribution function analysis. YVO$_3$ is a prototype for orbital ordering, exhibiting two consecutive transitions to *G*-type and *C*-type ordering with decreasing temperature. Evidence for local orbital ordering above the transition temperature of $T_{OO} \sim 200$ K is presented, obtained from the temperature dependence of the oxygen-oxygen octahedral correlations. This suggests that locally, *G*-type orbital ordering is present above the T_{OO} temperature but it is short range. With doping, it is expected that orbital ordering disappears altogether. By 30% of doping, as in Y$_{0.7}$La$_{0.3}$VO$_3$, even though no orbital ordering is expected, we find that locally, *C*-type orbital correlations are most likely present below the magnetic transition temperature T_N, allowing for a direct paramagnetic to orbitally ordered/antiferromagnetic transition in this composition.

I. INTRODUCTION

Transition-metal perovskite oxides exhibit unusual properties arising from strong electron-lattice interactions that can lead to orbital ordering [1], charge and spin stripe formation [2], polaron localization [3], Jahn-Teller (JT) distortions [4], and even phase separation. The insulating Y$_{1-x}$La$_x$VO$_3$, a JT active system, has been of considerable interest due to its complex phase diagram [5–13] associated with orbital physics [14–21]. With cooling, the parent compound, YVO$_3$, undergoes a transition to a *G*-type orbital ordering (antiphase ordering along the *c* axis, G-OO) at $T_{OO} \sim 200$ K, followed by a *C*-type antiferromagnetic spin ordering at $T_N \sim 116$ K (C-SO), and finally to an orbital flipping transition at $T_{CG} \sim 77$ K with *C*-type orbital ordering (in-phase ordering along the *c* axis, C-OO) and *G*-type spin ordering (G-SO) [19,22]. The transitions in the orbital and magnetic degrees of freedom are coupled with structural transitions. Above 200 K and below 77 K, the crystal symmetry is orthorhombic, while at intermediate temperatures, $77 < T < 200$ K, the symmetry is monoclinic [23]. For comparison, on the other end, in LaVO$_3$, the T_{OO} transition is suppressed, while the antiferromagnetic transition at $T_N \sim 143$ K is quickly followed by a structural transition ($T_t \sim 140$ K) from the orthorhombic to the monoclinic phase, the latter of which accommodates a G-OO/C-SO phase [24]. This state remains down to the lowest temperature where no orbital flipping transition is observed. Little is known of the suppression of T_{OO} and the disappearance of T_{CG} as a function of doping.

The V^{3+} *3d* orbitals are doubly degenerate in the t_{2g}^2 manifold. While the d_{xy} orbital is lower in energy and always occupied, the occupancy of the second orbital, d_{yz} or d_{xz}, alternates along the *c* axis. The alternating occupancy yields the *G*-type and *C*-type orbital patterns. This is best observed in the pure sample of YVO$_3$. Above T_{OO}, the crystal structure is orthorhombic with the *Pbnm* symmetry. In the temperature range between $T_{CG} < T < T_{OO}$, the structure is monoclinic with the $P2_1/a$ symmetry, while below T_{CG}, the system reenters the orthorhombic phase. The orbital patterns in the

two symmetries are shown in Figs. 1(a) and 1(b) [23], where in Fig. 1(a) the orbitals are in-phase along the *c* axis in the *Pbnm* symmetry, while in Fig. 1(b) the orbitals are out-of-phase in the $P2_1/a$ symmetry. Also shown in this figure is the spin orientation of Ti^{3+} ions. Above 200 K, no evidence for orbital ordering has been observed, suggesting that the orbitals are fluctuating. This is corroborated by thermal-conductivity measurements and Raman-scattering experiments [6,25,26] that unambiguously show that the orbitals are fluctuating above T_{OO} while some degree of orbital fluctuation is retained in the interval between $T_N < T < T_{OO}$. Complete static orbital order is only achieved below T_{CG}.

When YVO$_3$ is doped with La^{3+} as in Y$_{1-x}$La$_x$VO$_3$, it was previously shown that the T_{OO} transition is quickly suppressed and disappears by $x = 0.2$ [6]. Coupled with this suppression is the disappearance of the transition to the monoclinic phase as well, in the 77–200 K range, prior to reentering the orthorhombic phase. Beyond $x = 0.2$, only the orthorhombic phase is evident with the G-SO spin structure, in the absence of orbital ordering. At much higher doping levels, on approaching LaVO$_3$, G-OO/C-SO ordering reappears. It was earlier suggested that these phase transitions may be driven by the change in orbital ordering, following the JT pattern of distortion [27,28]. Thus solid solutions of Y$_{1-x}$La$_x$VO$_3$ provide an opportunity to investigate the disappearance of G-OO as a function of *x*, presumed to occur above $x \sim 0.2$, through the local structure.

The local atomic structure of Y$_{1-x}$La$_x$VO$_3$ $(0 < x < 0.30)$ was studied using neutron diffraction and the pair density function analysis. In YVO$_3$, evidence is provided that supports the presence of a local G-OO state above 200 K. The local symmetry above T_{OO} deviates from the expected average orthorhombic structure and it can be fit by a local model with a G-OO octahedral pattern. With doping, a sharp decline in the intensity of the local pair correlations is observed, especially above 3 Å at the lowest measured temperatures. This is brought about by the buckling and distortions of the VO$_6$ octahedra leading to a locally distorted structure. By 30%, the distortions
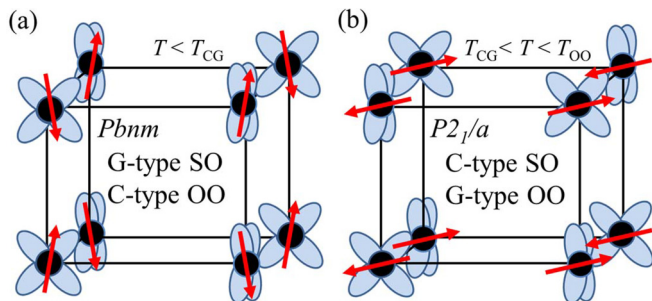
FIG. 1. (Color online) A schematic of the vanadium orbitals with C-type and G-type orbital ordering in YVO_3. (a) Below $T < 77$ K, the system has C-type orbital ordering (OO) and G-type spin ordering (SO). (b) For the temperature range of $77 < T < 200$ K, the system has G-type orbital ordering and C-type spin ordering in the monoclinic phase. The red arrows correspond to the spin direction.

observed locally reflect the presence of orbital ordering with a crossover transition around T_N resulting in a local G-SO, C-OO state.

II. EXPERIMENTAL DETAILS

Three single-phased $Y_{1-x}La_xVO_3$ ($0 \leqslant x \leqslant 0.3$) samples were melt grown using an image furnace following the procedure described elsewhere [29], with special attention given to prevent composition segregation. All samples were obtained by crushing single crystals into powders. The La^{+3} and Y^{+3} ions carry no moment, thus any observed magnetic signal arises from the V^{3+} ions. The isovalent substitution of La^{3+} for Y^{3+} allows for the study of the evolution of the transition temperature with the ionic radius at the A site without interference from a magnetic moment.

The powder neutron-diffraction experiment was carried out using the NOMAD diffractometer, which is a high-flux, medium-resolution diffractometer, at the Spallation Neutron Source (SNS) of the Oak Ridge National Laboratory [30]. The data were collected for 2.5 hours at each temperature. The average structure was determined by the Rietveld method [31] and the same diffraction data was normalized and Fourier transformed to get the pair density function (PDF). The Rietveld refinement provides a description of the average or long-range atomic arrangement, with reliable information of the unit-cell parameters, while the PDF provides information on the nature of local distortions that do not follow the lattice periodicity. This method has been applied successfully in many oxide systems [32–34]. The PDF is a real-space representation of the atomic correlations [35]. The diffraction data were corrected for instrumental background and sample containment, and normalized using a vanadium standard. The corrected data were used to obtain the total structure factor, $S(Q)$, where Q is the momentum transfer defined as $Q = 4\pi \sin\theta/\lambda$ and a $Q_{max} \sim 40 \, \text{Å}^{-1}$ was used. The $S(Q)$ is Fourier transformed to obtain the PDF, $\rho(r)$, defined as follows:

$$\rho(r) = \rho_0 + \frac{1}{2\pi^2 r} \int Q(S(Q) - 1)\sin(Qr)dQ,$$

where ρ_0 is the average atomic number density. Data were collected between 5 and 300 K. Vanadium has a small

neutron-scattering length and is negative as well. Thus correlations involving vanadium are negative given that the amplitude of the PDF peaks is normalized with the scattering length as well as the concentration of atoms in the unit cell.

III. RESULTS

A. The structure of YVO_3

The temperature dependence of the lattice parameters obtained from the Rietveld refinement is listed in Table I. The $P2_1/a$ setting rather than the standard $P2_1/c$ was chosen in order to retain the double perovskite structure along the c axis. In Fig. 2(a), the PDFs corresponding to the local structure of YVO_3 at several temperatures are plotted up to 5 Å. The first negative peak corresponds to the V-O correlations, i.e., the shortest pair correlation in the perovskite unit cell. This peak, and any peak that includes V, is small in intensity because of the small coherent neutron cross section of the vanadium ion. Following are Y-O and O-O correlations. Given the weak scattering from vanadium, it is mostly Y and O correlations that contribute to the total PDF. As can be seen from the figure, differences are observed in the local structure of YVO_3 as a function of temperature, especially above 150 K, and are discussed below.

At the lowest measured temperature, the average crystal symmetry is orthorhombic. A model PDF is calculated using the atomic coordinates and unit-cell dimensions obtained from the Rietveld refinement of the orthorhombic cell. The model PDF is a linear combination of all of the partial functions calculated for each pair of atoms assuming a Gaussian distribution, and normalized by the concentration and scattering lengths [32]. The comparison of the model PDF for the orthorhombic symmetry (solid line) yields a very good agreement with the experimental data (symbols) corresponding to the local structure at 5 K, as shown in Fig. 2(b). Also shown in this figure is the difference between the model and data.

Upon warming, the structure undergoes a transition to the monoclinic symmetry, $P2_1/a$, in the $77 < T < 200$ K temperature range. The data at 200 K is compared to a model PDF calculated using the $P2_1/a$ atomic coordinates and unit-cell dimensions [Fig. 2(c)]. Although the overall agreement is good between the two, several differences are observed that cannot be reproduced using the average structure model. Also shown in this figure is a comparison between the same data at 200 K and a local model that fits the data well.

TABLE I. The temperature dependence of the lattice parameters in YVO_3. The temperature dependence of the crystal symmetry is consistent with previous measurements.

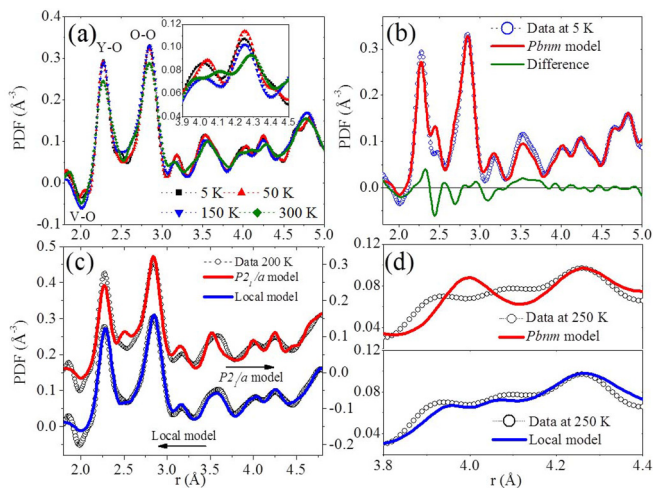| T (K)	Space group	a (Å)	b (Å)	c (Å)	Vol (Å^3)
300	$Pbnm$	5.6111(1)	7.5838(2)	5.2847(1)	224.88(1)
250	$Pbnm$	5.6115(1)	7.5783(2)	5.2822(1)	224.68(1)
200	$P2_1/a$	5.2803(2)	7.5709(2)	5.6117(2)	224.34(1)
150	$P2_1/a$	5.2735(1)	7.5435(3)	5.6053(2)	222.98(1)
50	$Pbnm$	5.5946(1)	7.5612(2)	5.2869(1)	223.65(1)
5	$Pbnm$	5.5940(2)	7.5603(2)	5.2866(2)	223.58(2)

FIG. 2. (Color online) The temperature dependence of the local structure of YVO$_3$. (a) Four PDFs. Inset: An enlarged region of the local structure between 3.9 and 4.5 Å. (b) The data at 5 K is fit using the parameters for the orthorhombic average structure. (c) The 200 K data is fit using two models: comparison with the average monoclinic structure (upper) and comparison with a local structure (lower). (d) The 250 K data in the range shown is compared to two models: comparison with the average *Pbnm* (upper) and comparison with a local model that is modified from the monoclinic symmetry (lower).

The local model follows the monoclinic symmetry constraints but with the oxygen coordinates refined further to fit the short-range structure.

Above 200 K, the crystal structure reenters the orthorhombic phase. A comparison of the data at 250 K with a model PDF assuming the orthorhombic symmetry shows that a mismatch exists between the average structure and the local structure. This is most prominently demonstrated in the 3.8–4.4 Å range shown in the upper panel of Fig. 2(d). In this, the data displays a three-peak structure that cannot be reproduced by the model calculated based on the orthorhombic symmetry. This region corresponds to O-O and Y-O correlations in real space. To reproduce this structure, it requires that the monoclinic symmetry be used, which indicates that locally the symmetry remains $P2_1/a$ above T_{OO}, even though globally it is orthorhombic. The three-peak structure is evident in the 200 K data shown as well, but the split is smaller at this temperature. Thus, even though T_{OO} marks the temperature of the orbital order to disorder transition, the local atomic order does not follow the global structural order.

What is responsible for the differences observed between the data and the average structure? The answer lies in the oxygen correlations. To reproduce the distorted structure observed between 3.8–4.4 Å, a local model is used in which the oxygen site symmetry is broken as in the monoclinic symmetry. The fitting shown in the lower panel of Fig. 2(d) is quite good up to 5 Å, but for longer distances, the fitting breaks down, which suggests that the proposed distortion pattern does not propagate in the long-range structure, but is local, within the unit cell. It is only when it becomes long range that the symmetry would change to monoclinic globally with cooling.

Table II is a complete list of the O-O and the Y-O bond lengths that contribute to this region in space at 200, 250,

TABLE II. The results from the local structure refinement of the experimental data of YVO$_3$ at three temperatures. Listed are the O-O and Y-O correlations in the 3.8–4.4 Å range. The subscripts $(a + b)$ and $(a - b)$ indicate the directions of the O-O bonds. The Y-O bonds are the closest correlations to the O-O correlations.

T (K)	O(1)-O(1)$_c$	O(2)-O(2)	O(3)-O(3)	Y-O pairs (Å)
200	4.040(37)	4.016(62)$_{(a+b)}$	4.102(62)$_{(a+b)}$	4.208(59)
	3.949(38)	4.119(64)$_{(a-b)}$	3.929(65)$_{(a-b)}$	4.220(42)
250	3.954(37)	4.172(64)$_{(a+b)}$	3.920(62)$_{(a+b)}$	4.149(43)
	4.056(37)	3.916(66)$_{(a-b)}$	4.091(65)$_{(a-b)}$	4.199(57)
300	4.119(38)	4.148(66)$_{(a+b)}$	3.964(62)$_{(a+b)}$	4.156(30)
	3.968(38)	4.021(63)$_{(a-b)}$	4.011(60)$_{(a-b)}$	4.276(44)

and 300 K. The local structure described above implies that an orbital pattern exists even above T_{OO} that is locally very similar to the one observed in the $T_{CG} < T < T_{OO(=200K)}$ temperature range. Shown in Fig. 3(a) is a schematic of the *ab* plane of the VO$_6$ octahedra where only oxygen-oxygen bond lengths are indicated. The values are obtained from the local model fitting of the data at 250 K. For simplicity, a pseudocubic unit cell is chosen for the representation. The $z = 0$ and $z = 0.5$ are plotted because of the nature of the orbital pattern which alternates along the *c* axis. The long and short O-O bonds in Fig. 3(a) follow the *G*-type orbital pattern indicated in Fig. 3(b). Plotted in gray are the orbitals of $3d_{xy}$ which are always occupied. Superimposed are the orbitals of $3d_{xz}$ and $3d_{yz}$ which alternate occupancy along the *c* axis. These findings serve as evidence for local *G*-type orbital ordering above T_{OO}.

B. The structure of Y$_x$La$_{1-x}$VO$_3$

With doping, *G*-type orbital and *C*-type spin ordering gradually disappear and the gap in $T_{CG} < T < T_{OO}$ closes. Above $x = 0.20$, no evidence has been observed to support the presence of a G-OO/C-SO state, while a transition from
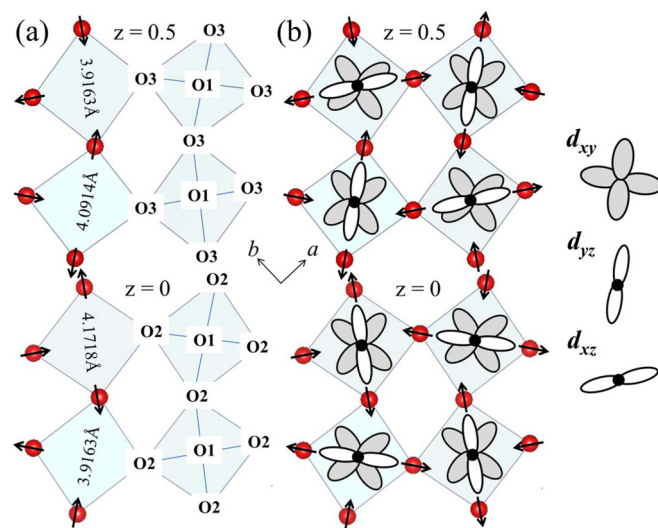

FIG. 3. (Color online) A schematic diagram of the VO$_3$ octahedra in YVO$_3$ in the *ab* plane at $z = 0$ and $z = 0.5$. (a) Only bond lengths between O-O correlations are shown. The arrows indicate direction of displacement. The short and long O-O pairs are stacked alternately along the *c* axis. (b) The expected orbital pattern is shown.
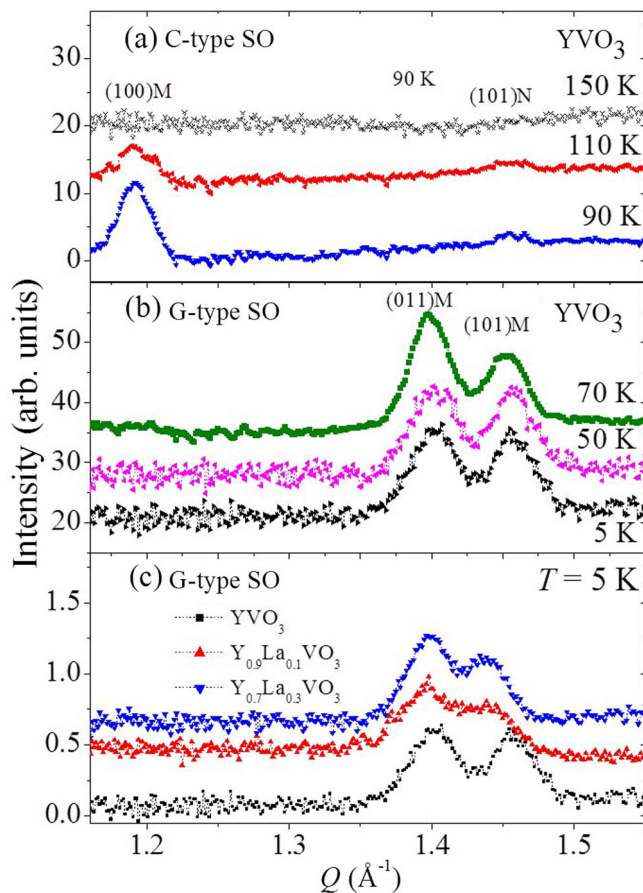
FIG. 4. (Color online) The magnetic Bragg peaks in (a) are due to C-type spin ordering with $T_N = 116$ K. (b) G-type spin ordering appears below $T_{CG} = 77$ K. (c) G-type spin ordering is observed in all three compositions at $T = 5$ K.
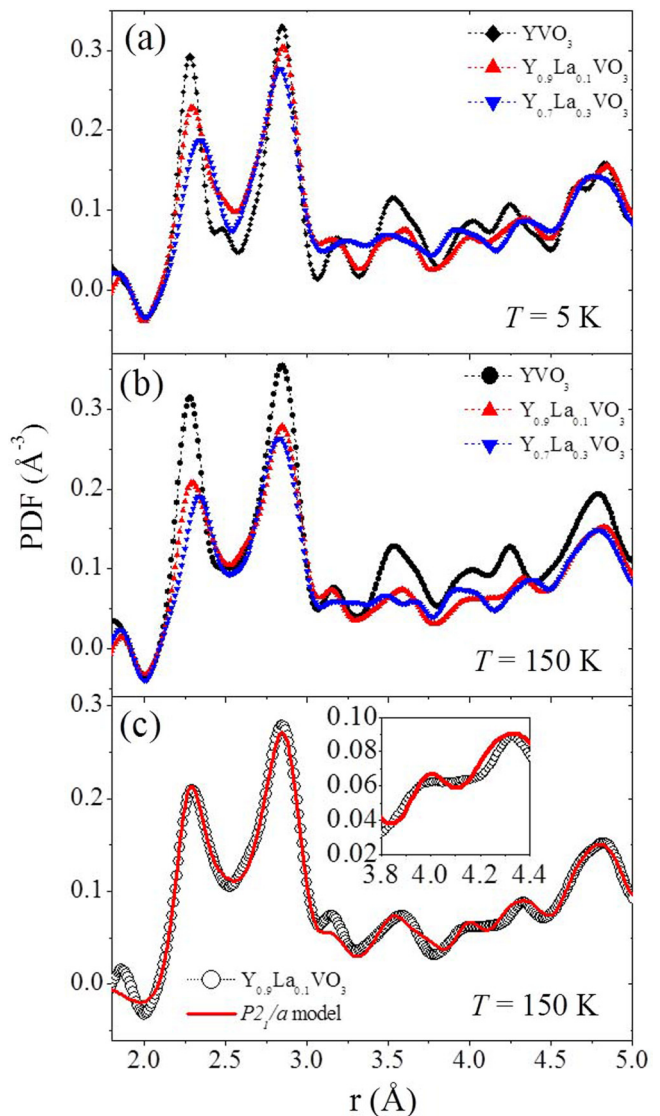

FIG. 5. (Color online) The composition dependence of the local structure is shown at two temperatures: (a) $T = 5$ K and (b) $T = 150$ K. (c) The data of the 10% composition at 150 K is fit using the monoclinic $P2_1/a$ average structure.

the low-temperature C-OO/G-SO to an orbitally disordered and paramagnetic state occurs instead. The absence of the G-OO state with doping also corresponds to the absence of the C-SO magnetic phase above $x = 0.20$. Coupled with this is the absence of the monoclinic structure phase in the intermediate-temperature regime.

The magnetic diffraction pattern and its composition dependence shown in Fig. 4 are in agreement with the structure previously reported [19]. Upon cooling, the C-SO phase appears below 116 K in the parent composition, YVO$_3$, evidenced by the presence of the (100) magnetic peak [Fig. 4(a)]. At 77 K, a spin-flip transition to the G-SO magnetic state occurs and two magnetic peaks are most prominent, the (011) and (101), as shown in Fig. 4(b). Very little difference is observed in the $x = 0.1$ composition, which indicates that the magnetic structure is the same as in the pure sample. By $x = 0.3$, however, only the low-temperature G-SO magnetic structure is present [Fig. 4(c)].

With doping, the local structure changes in significant ways, as can be seen from Figs. 5(a) and 5(b), which are plots of the PDF's corresponding to the local structures for the three compositions at 5 and 150 K, respectively. At 5 K, even though the average symmetry is orthorhombic in all three, clearly the local structure changes as a function of La doping that

cannot be accounted for by substituting the bigger La atom for Y. The substitution of the larger La for Y leads to an expansion of the lattice and a shift of the PDF peaks to the right. Locally, however, the correlation peaks become very broad and lose their intensity. A similar observation is made at 150 K, at which temperature a structural phase transition to the monoclinic phase occurs in the $x = 0.0$ and 0.10, but not in the $x = 0.3$. It can also be observed from Figs. 5(a) and 5(b) that the shape of the first negative PDF peak that corresponds to V-O pair correlations does not change with doping, which indicates that the octahedron remains rigid. At the same time, the suppression of the intensity and broadening of the peak correlations, especially above 3 Å, indicate significant loss of the coherence of the correlations. This striking change is mostly observed within 5 Å.

In Fig. 5(c), the data of the $x = 0.10$ composition at 150 K is compared to a model calculated from the average monoclinic
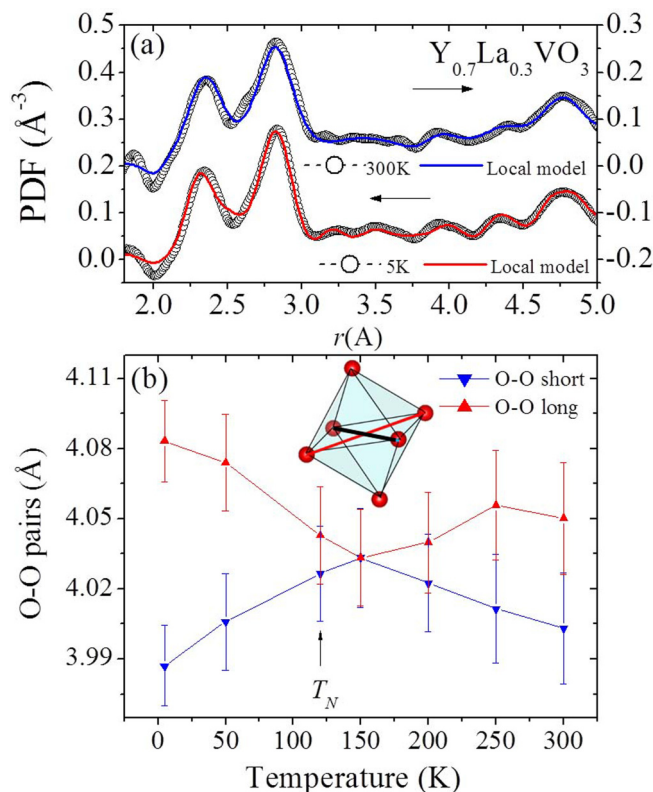
FIG. 6. (Color online) (a) The data for $Y_{0.7}La_{0.3}VO_3$ at two temperatures are fit using a local model that is refined based on the *Pbnm* coordinates. (b) The bond lengths of O-O pairs around 4.0 Å are obtained from the refined unit cell. The O-O bonds split to short and long below T_N.

TABLE III. The temperature dependence of the local bond lengths of O-O correlations in $x = 0.30$. The values are given in angstroms.

T (K)	O(1)-O(1)	O(2)-O(2)$_{short}$	O(2)-O(2)$_{long}$
5	4.014(7)	3.987(17)	4.083(17)
50	3.989(9)	4.006(21)	4.074(21)
120	4.015(9)	4.027(20)	4.042(21)
150	4.018(9)	4.033(21)	4.033(21)
200	4.013(10)	4.022(21)	4.040(21)
250	4.019(9)	4.016(23)	4.056(24)
300	4.018(10)	4.003(24)	4.050(24)

are split but the split is smaller, as seen in the figure. It can also be seen in the 300 K data of Fig. 6(a) that the correlations have smeared out significantly, making it harder to distinguish between the short and long pairs. The loss of coherence of the (Y,La)-O affects the orbital ordering state of this system via the A-O covalency [36]. Given that the *A*-site ions are involved, *A*-site pair correlations are also smeared.

IV. SUMMARY

The local structure of $Y_{1-x}La_xVO_3$ has been investigated using neutron scattering and the pair density function analysis technique. The phase diagram shown in Fig. 7 summarizes our results. In YVO$_3$, local *G*-type orbital order is most likely present above $T_{OO} = 200$ K, where the local structure favors a modified $P2_1/a$ symmetry and *G*-type orbital ordering. Since the local *G*-type orbital order is present at room temperature, the system naturally turns into a *G*-type orbital ordering state at $T = 200$ K. By doping La^{3+} at the Y site and by decreasing temperature, the system loses the G-OO state. *G*-type orbital ordering disappears at $Y_{0.7}La_{0.3}VO_3$. Our analysis suggests that C-OO is most likely present in $Y_{0.7}La_{0.3}VO_3$, as discussed above. From specific-heat measurements on the

structure. The $x = 0.10$ is very similar to the parent compound, with its T_{OO} transition suppressed down to 170 K. On the other hand, its T_{CG} increases to 98 K. The fitting to the monoclinic symmetry which corresponds to the G-OO phase is quite good. However, just like in the case of the pure sample [see Fig. 2(c)], it cannot reproduce the splitting of the correlations in the 3.8 to 4.4 Å range. Just like in the parent compound, a local model needs to be implemented where the oxygen coordinates are refined further to fit the short-range structure.

By $x = 0.30$, the smearing of the PDF peaks in the data is quite distinct [see Fig. 5(a)]. At this composition, no orbital ordering is expected. Is there evidence for local orbital ordering at this composition? In Fig. 6(a), the data at 300 and 5 K are compared to models calculated from the constraints of the orthorhombic symmetry, but with the parameters refined to fit the data. We focus on the O-O octahedral correlations as in YVO$_3$. Shown in Fig. 6(b) is the temperature dependence of the oxygen pairs which represent short and long O-O bonds, as indicated in the inset. In the *Pbnm* symmetry, the stacking along the c axis does not change, implying that the same orbital pattern exists along the c axis as in the pure YVO$_3$. This suggests that *local C*-type orbital ordering is present in $Y_{0.7}La_{0.3}VO_3$ below 120 K. Below $T_N \sim 120$ K, the spin ordering favors orbital ordering, leading to a large separation of the O-O bond distances. Table III provides a list of the local O-O bond lengths as a function of temperature from fitting the data using the local model. Above this temperature, the bonds
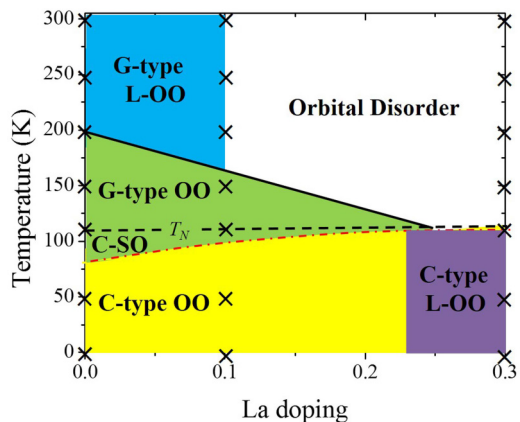

FIG. 7. (Color online) The phase diagram of $Y_{1-x}La_xVO_3$. The crosses correspond to the temperature points that were collected. L-OO designates the presence of local orbital ordering. This appears above T_{OO} in the 0 and 10% compositions and below T_N in the 30%.

$Y_{0.9}La_{0.1}VO_3$ [6] and $Y_{0.7}La_{0.3}VO_3$ [37], it was suggested that there exist three phase transitions, namely, orbital ordering, antiferromagnetic, and orbital flipping transitions in $Y_{0.9}La_{0.1}VO_3$, but only one transition to an antiferromagnetic phase in $Y_{0.7}La_{0.3}VO_3$. Combined with our data, it is suggested that in $Y_{0.7}La_{0.3}VO_3$, the system transforms from a paramagnetic state to C-OO/G-SO which resembles $LaVO_3$. Future plans will include extending this work to $LaVO_3$ by further doping $Y_{1-x}La_xVO_3$.

[1] Y. Tokura and N. Nagaosa, Science **288**, 462 (2000).

[2] J. M. Tranquada, in *Neutron Scattering in Layered Copper-Oxide Superconductors*, edited by A. Furrer (Kluwer Academic, Dordrecht, 1998).

[3] P. Tong, J. Yu, Q. Huang, K. Yamada, and D. Louca, Phys. Rev. Lett. **106**, 156407 (2011).

[4] K. I. Kugel and D. I. Khomskii, Sov. Phys. Usp. **25**, 231 (1982).

[5] Y. Ren, T. T. M. Palstra, D. I. Khomskii, E. Pellegrin, A. A. Nugroho, A. A. Menovsky, and G. A. Sawatzky, Nature (London) **396**, 441 (1998).

[6] J.-Q. Yan, J.-S. Zhou, J. G. Cheng, J. B. Goodenough, Y. Ren, A. Llobet, and R. J. McQueeney, Phys. Rev. B **84**, 214405 (2011).

[7] J.-Q. Yan, J.-S. Zhou, J. B. Goodenough, Y. Ren, J. G. Cheng, S. Chang, J. Zarestky, O. Garlea, A. Llobet, H. D. Zhou, Y. Sui, W. H. Su, and R. J. McQueeney, Phys. Rev. Lett. **99**, 197201 (2007).

[8] J.-S. Zhou, J. B. Goodenough, J.-Q. Yan, and Y. Ren, Phys. Rev. Lett. **99**, 156401 (2007).

[9] G. Khaliullin, P. Horsch, and A. M. Oleś, Phys. Rev. Lett. **86**, 3879 (2001).

[10] T. N. De Silva, A. Joshi, M. Ma, and F. C. Zhang, Phys. Rev. B **68**, 184402 (2003).

[11] D. Bizen, K. Nakatsuka, T. Murata, H. Nakao, Y. Murakami, S. Miyasaka, and Y. Tokura, Phys. Rev. B **78**, 224104 (2008).

[12] D. Bizen, H. Nakao, K. Iwasa, Y. Murakami, T. Osakabe, J. Fujioka, T. Yasue, S. Miyasaka, and Y. Tokura, J. Phys. Soc. Jpn. **81**, 024715 (2012).

[13] Z. Fang and N. Nagaosa, Phys. Rev. Lett. **93**, 176404 (2004).

[14] M. Noguchi, A. Nakazawa, S. Oka, T. Arima, Y. Wakabayashi, H. Nakao, and Y. Murakami, Phys. Rev. B **62**, R9271(R) (2000).

[15] J. Reul, A. A. Nugroho, T. T. M. Palstra, and M. Grüninger, Phys. Rev. B **86**, 125128 (2012).

[16] M. De Raychaudhury, E. Pavarini, and O. K. Andersen, Phys. Rev. Lett. **99**, 126402 (2007).

[17] P. Horsch, G. Khaliullin, and A. M. Oleś, Phys. Rev. Lett. **91**, 257203 (2003).

[18] S. Sugai and K. Hirota, Phys. Rev. B **73**, 020409(R) (2006).

[19] C. Ulrich, G. Khaliullin, J. Sirker, M. Reehuis, M. Ohl, S. Miyasaka, Y. Tokura, and B. Keimer, Phys. Rev. Lett. **91**, 257202 (2003).

[20] E. Benckiser, R. Rückamp, T. Möller, T. Taetz, A. Möller, A. A. Nugroho, T. T. M. Palstra, G. S. Uhrig, and M. Grüninger, New J. Physics **10**, 053027 (2008).

[21] D. A. Mazurenko, A. A. Nugroho, T. T. M. Pelstra, and P. H. M. van Loosdrecht, Phys. Rev. Lett. **101**, 245702 (2008).

[22] K. Kawano, H. Yoshizawa, and Y. Ueda, J. Phys. Soc. Jpn. **63**, 2857 (1994).

[23] G. R. Blake, T. T. M. Palstra, Y. Ren, A. A. Nughoho, and A. A. Menovsky, Phys. Rev. Lett. **87**, 245501 (2001); Phys. Rev. B **65**, 174112 (2002).

[24] P. Bordet, C. Chaillout, M. Marezio, Q. Huang, A. Santoro, S.-W. Cheong, H. Takagi, C. S. Oglesby, and B. Batlogg, J. Solid. State. Chem. **106**, 253 (1993).

[25] S. Miyasaka, Y. Okimoto, M. Iwama, and Y. Tokura, Phys. Rev. B **68**, 100406(R) (2003).

[26] A. A. Tsvetkov, F. P. Mena, P. H. M. van Loosdrecht, D. van der Marel, Y. Ren, A. A. Nugroho, A. A. Menovsky, I. S. Elfimov, and G. A. Sawatzky, Phys. Rev. B **69**, 075110 (2004).

[27] H. Sawada, N. Hamada, K. Terakura, and T. Asada, Phys. Rev. B **53**, 12742 (1996).

[28] H. Sawada and K. Terakura, Phys. Rev. B **58**, 6831 (1998).

[29] J.-Q. Yan, J.-S. Zhou, and J. B. Goodenough, Phys. Rev. Lett. **93**, 235901 (2004).

[30] J. Neuefeind, M. Feygenson, J. Carruth, R. Hoffmann, and K. K. Chipley, Nucl. Instr. Meth. Phys. Res. B **287**, 68 (2012).

[31] A. C. Larson and R. B. Von Dreele, Los Alamos National Laboratory Report No. LAUR 86-748, 1994 (unpublished).

[32] D. Louca and T. Egami, Phys. Rev. B **59**, 6193 (1999).

[33] B. H. Toby and T. Egami, Acta Crystall. A **48**, 336 (1992).

[34] D. Louca, T. Egami, E. L. Brosha, H. Röder, and A. R. Bishop, Phys. Rev. B **56**, R8475(R) (1997).

[35] B. E. Warren in *X-ray Diffraction* (Dover, New York, 1990).

[36] T. Mizokawa, D. I. Khomskii, and G. A. Sawatzky, Phys. Rev. B **60**, 7309 (1999).

[37] J.-Q. Yan *et al.* (unpublished).